Applied Clay Science 87 (2014) 245–253

Contents lists available at ScienceDirect

Applied Clay Science

journal homepage: www.elsevier.com/locate/clay

Research paper

Effect of the Al/clay ratio on the thiabendazol removal by aluminum pillared clays

M. Eugenia Roca Jalil [a,b], Miria Baschini [b], Enrique Rodríguez-Castellón [c], Antonia Infantes-Molina [d], Karim Sapag [a,*]

[a] Laboratorio de Sólidos Porosos, Instituto de Física Aplicada, CONICET — Universidad Nacional de San Luis, Chacabuco 917, CP 5700 San Luis, Argentina
[b] Laboratorio de Arcillas, Facultad de Ingeniería, Universidad Nacional del Comahue, Buenos Aires 1400, 8300 Neuquén, Argentina
[c] Departamento de Química Inorgánica, Cristalografía y Mineralogía, Facultad de Ciencias, Universidad de Málaga, Campus de Teatinos s/n, 29071 Málaga, Spain
[d] Instituto de Catálisis y Petroleoquímica, CSIC, Cantoblanco, 28049 Madrid, Spain

ARTICLE INFO

Article history:
Received 9 May 2013
Received in revised form 6 November 2013
Accepted 8 November 2013
Available online 28 November 2013

Keywords:
Fungicide adsorption
Thiabendazole
Aluminum pillared clay
Adsorbents

ABSTRACT

In this work, four aluminum pillared clays (Al-PILC) with different Al/clay ratios were synthesized and evaluated for the removal of thiabendazole (TB) (a fungicide widely used in agricultural activities) from aqueous media. The Al-PILC were thoroughly characterized by different techniques, such as X-ray diffraction (XRD), thermogravimetric analysis (DTA-TG), adsorption–desorption of N_2 at 77 K, NH_3-temperature programmed desorption (NH_3-TPD) and transmission electron microscopy (TEM). The TB-adsorption studies were carried out in batch, at room temperature, at pH = 6 (natural pH, without additional control) and with different concentrations of TB (2–100 ppm). The measured TB adsorption capacities varied from 11.78 to 17.50 mg TB per gram of clay. The TB–Al PILC complexes obtained after the adsorption process were studied by X-ray photoelectron spectroscopy (XPS). The results suggested that the molecules of TB were adsorbed on the Al-PILC by two different phenomena: by physisorption in their porous structure and by chemisorption on their pillars, showing a concordance between the amounts of incorporated aluminum in the pillared clays and their fungicide adsorption capacity.

1. Introduction

During the last years, the presence of organic compounds as pesticides, antibiotics, hormones and dyes in the environment has become a matter of growing interest. Pesticides have been found in soils and watercourses as a result of agricultural practices. The majority of these pesticides are not biodegradable and their adsorption from solution has been proven to be a feasible methodology to remove these pesticides from aqueous courses.

Many natural adsorbents have been studied; among them, the natural clay minerals are a good option because of their abundance. Natural clay minerals have showed optimal adsorption capabilities with various organic and inorganic pollutants due to their surface area and their cation-exchange capacity (Crini, 2006). However, these materials are highly hydrophilic and their separation from aqueous dispersions is difficult. In consequence, additional techniques like flocculation are required to separate these adsorbents from aqueous media.

The pillared interlayered clay minerals (PILC) are laminar solids with a permanent porous structure commonly obtained from natural clay minerals as montmorillonite (Mt). These materials are synthesized through a cationic exchange process that involves the displacement of the cations from the natural material by hydroxyl-metal polycations. After a thermal treatment, polycations become oxide species within the interlayer, keeping the layers separated and avoiding the collapse of the structure, such oxides are the so-called pillars of the PILC. The pillars provide new acid sites to the material and a permanent microporous structure within the interlayer that produces a considerable increase of the specific surface area (Cool and Vansant, 1998; Gil et al., 2008; Kloprogge, 1998; Vicente et al., 2013). The studies with PILC began during the oil crisis in the 70's as optional catalysts to zeolites. Nowadays, due to their features, the PILC are used as catalysts or catalyst support in several reactions (Gil et al., 2008; Oliveira et al., 2008; Romero-Pérez et al., 2012; Vicente et al., 2013) and as adsorbents for organic (Gil et al., 2011; Hou et al., 2011; Konstantinou et al., 2000; Molu and Yurdakoc, 2010; Polubesova et al., 2002) and inorganic (Manohar et al., 2005; Tian et al., 2009) pollutants.

The adsorption mechanism of different organic compounds from aqueous solution on natural clay minerals is generally related to cation exchange or van der Waals interactions (Wang et al., 2011). In particular, previous studies have shown that TB adsorption is related to cation exchange of the protonated fungicide by the interlayer cations of the

* Corresponding author at: Chacabuco 917, CP 5700 San Luis, San Luis, Argentina. Tel./fax: +54 2664436151.
E-mail addresses: merocajalil@gmail.com (M.E. Roca Jalil), miria.baschini@fain.uncoma.edu.ar (M. Baschini), castellon@uma.es (E. Rodríguez-Castellón), ainfantes@icp.csic.es (A. Infantes-Molina), sapag@unsl.edu.ar (K. Sapag).

0169-1317/$ – see front matter © 2013 Elsevier B.V. All rights reserved.
http://dx.doi.org/10.1016/j.clay.2013.11.014

natural clay mineral (Lombardi et al., 2003, 2006). However, in Al-PILC the interlayer cations of the natural clay mineral were replaced by aluminum oligocations, which are transformed into pillars of aluminum oxides when they are subjected to thermal treatment. These aluminum pillars can give rise to different adsorption mechanisms of organic species on PILC. In fact, PILC have two main differences with natural clay mineral: the porous structure and the presence of acid surface sites. The porous structure is important because it can give rise to steric effects depending on the adsorptive molecular size as was showed by Mishael et al. (1999). In addition, the presence of aluminum in the pillars produces new Lewis acid sites that can contribute to the adsorption of organic molecules with Lewis basic character (Undabeytia et al., 2000). In spite of the fact that PILC are widely studied as adsorbents, there are a few exhaustive studies about the concordance between their porous structure and their removal capacity.

Thiabendazole (TB) is a fungicide widely used in the production of different species such as sugar cane, tobacco, rice, apple and other products, as well as a post-harvest fungicide before fruit packing. The *Alto Valle de Río Negro-Neuquén* region (Argentine) is the major producer of apples and pears of the country. In this region, TB is one of the most used post-harvest fungicides and is found in the main waterways, where its concentration is superior to the advisable values for drinking water. Although thiabendazole does not have a high risk of toxicity, its accumulation in the environment causes the increasing resistance of some microorganisms. A previous study has showed that natural clays, abundant in this region, are suitable as TB adsorbents in spite of the inconveniences mentioned above (Lombardi et al., 2003). Recently, Roca Jalil et al. (2013) reported an aluminum PILC (synthesized from one of these natural clay minerals) as TB adsorbent in aqueous medium, obtaining better TB adsorption capacities than the former natural clay mineral with the advantage of being more easily separated from the adsorption medium due to its hydrophilicity.

In this work, four aluminum PILC (Al-PILC) with different Al–clay ratios were synthesized and characterized by different techniques. Their structural, textural and surface properties were contrasted with their TB removal capacity, in order to establish a relationship between the Al-PILC properties and TB adsorption. Also, the adsorbate–adsorbent interaction was studied by XPS, with the aim of proposing a possible mechanism of TB adsorption on PILC materials.

2. Materials and methods

2.1. Synthesis of materials

The natural clay used in this work is a bentonite from the Pellegrini Lake, in *Rio Negro* province, Argentina. This clay has been described in a previous work (Roca Jalil et al., 2013). The PILC were prepared following the previously described methodology in which the oligocations were synthesized from a 0.2 M of $AlCl_3 \cdot 6H_2O$ solution and 0.5 M of NaOH solution, with a basicity relationship $OH^-/Al^{3+} = 2$, under stirring at 60 °C (Roca Jalil et al., 2013; Sapag and Mendioroz, 2001). The resultant solutions were aged under stirring for 12 h at room temperature and the oligocation obtained was added drop wise to a 3 mass% dispersion of natural clay in deionized water. Four PILC were prepared with different quantities of aluminum: 5, 10, 15 and 20 meq of aluminum per gram of clay, according to previous work (Romero-Pérez et al., 2012). The samples were washed using dialysis membranes until no chloride ions were found. Subsequently, the precursors obtained were dried at 60 °C and calcined at 500 °C for 1 h, with a heating rate of 10 °C min^{-1}. The PILC obtained were named: *Al-PILC 5*, *Al-PILC 10*, *Al-PILC 15* and *Al-PILC 20*, respectively.

2.2. Adsorptive: thiabendazole (TB)

A product commercialized as TECTO by Syngenta where the active agent is the TB in a 48.5% mass/mass aqueous dispersion, was used as adsorptive for the adsorption studies. The TB has a molecular mass of 201.3 g mol^{-1} and its solubility in water is 0.16 g L^{-1} at pH 4 and 0.03 g L^{-1} at pH 7–10, both at 20 ± 0.5 °C (Tway and Love, 1982). The dimensions of the TB molecule are 9.89 Å of length and 4.97 Å of width, estimated by using the software Gaussian03Rw. The TB thickness is below 2 Å due to this molecule is flat (Lombardi et al., 2003; Roca Jalil, 2010). TB has three pK_a values in aqueous solution, which are 2.5, 4.7 and 12.0; four different species can be generated by protonation–deprotonation reactions according to the pH of the solution. The molecular structure of TB and the protonated–deprotonated species are shown in Fig. 1. Fig. 2 shows the distribution of TB species at different pH obtained with the method reported by Del Piero et al. (2006).

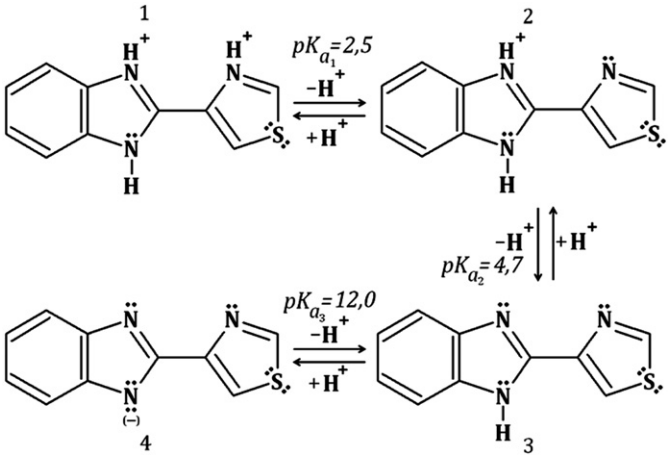

Fig. 1. Protonated–deprotonated species of TB.

2.3. Characterization of the adsorbents

Structural properties were analyzed by X-ray diffraction (XRD) using a RIGAKU Geigerflex X-ray diffractometer with Cu Kα radiation at 20 mA and 40 kV. The scans were recorded between 2° and 70° (2θ) with a step size of 0.02° and a scanning speed of 2°min^{-1}. Thermogravimetric analyses (TGA) were performed using a Shimadzu TG-51 equipment. The analyses were carried out by heating approximately 0.015 g of sample up to 1000 °C with a rate of 10 °C min^{-1}, in a dynamic air atmosphere.

Textural properties were obtained from nitrogen adsorption–desorption isotherms at 77 K using an ASAP 2000 (*Micromeritics*

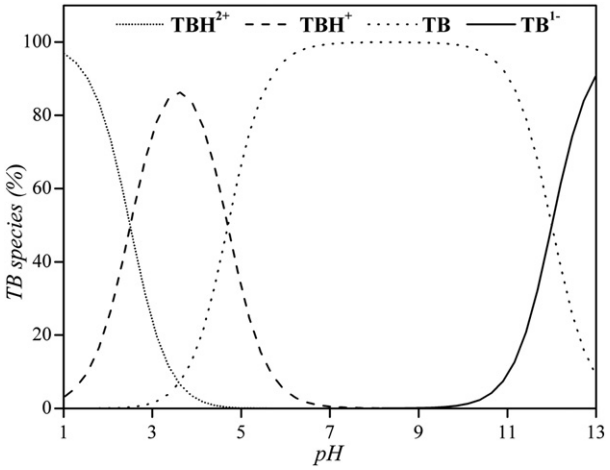

Fig. 2. Distribution of TB species as a function of pH.

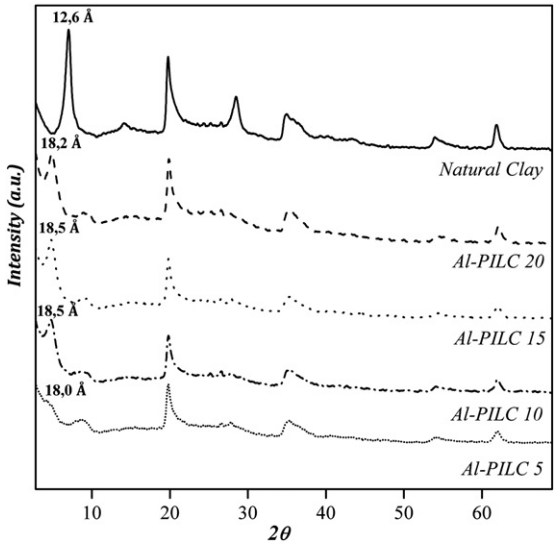

Fig. 3. XRD patterns of natural and PILC.

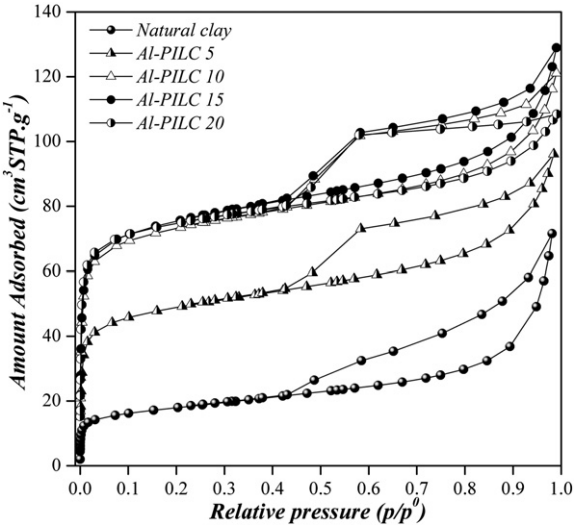

Fig. 5. N_2 adsorption–desorption isotherms at 77 K for natural and PILC.

Instruments) manometric equipment. Prior to each analysis, the samples were degassed for 12 h at 200 °C under vacuum. The specific surface area (S_{BET}) was assessed by the Brunauer, Emmet and Teller (BET) method. The micropore volumes ($V_{\mu p}$) were calculated with the *α-plot* method using as a reference material the natural clay calcined at 800 °C. The total pore volume (V_T) was obtained using the Gurvich rule (at 0.97 of relative pressure) (Rouquerol et al., 1999). Pore size distributions (PSD) were obtained by the Horvath–Kawazoe method, considering the adsorption branch and that the PILC have slit shape pores within the interlayer region.

The surface acidity was determined by ammonia thermo-programmed desorption (NH_3-TPD). The equipment was previously calibrated by measuring the corresponding signals of the thermal decomposition of known amounts of hexaamminenickel (II) chloride $[Ni(NH_3)_6]Cl_2$, supplied by Aldrich. The analyses were carried out in a tubular reactor with 0.080 g of adsorbent. Before the analysis, the samples were cleaned under an inert atmosphere (He, 35 mL min^{-1}), heating from room temperature up to 550 °C for 10 min, and then cooling to 100 °C. The adsorption of ammonia was carried out for 5 min at this temperature and the physisorbed ammonia was eliminated by a He flow (35 mL min^{-1}). The desorption was performed by heating the samples from 100 °C to 550 °C at a heating rate of 10 °C min^{-1}. The ammonia desorbed was analyzed and quantified by an on-line gas chromatograph (Shimadzu GC-14A) equipped with a TCD.

Transmission electron micrographs of the adsorbents were obtained using a Philips CM 200 Supertwin-174 DX4 microscope. Samples were dispersed in ethanol and a drop of the dispersion was put on a Cu grid (300 mesh).

XPS spectra were collected using a physical electronics PHI 5700 spectrometer with non-monochromatic Mg Kα radiation (300 W, 15 kV, and 1486.6 eV) with a multi-channel detector. Spectra of the samples were recorded in the constant pass energy mode at 29.35 eV, using a 720 μm diameter analysis area. Charge referencing was measured against adventitious carbon (C 1*s* at 284.8 eV). A PHI ACCESS ESCA-V6.0 F software package was used for acquisition and data analysis. A Shirley-type background was subtracted from the signals. Recorded spectra were always fitted using Gaussian–Lorentzian curves in order to determine the binding energies of the different element core levels more accurately.

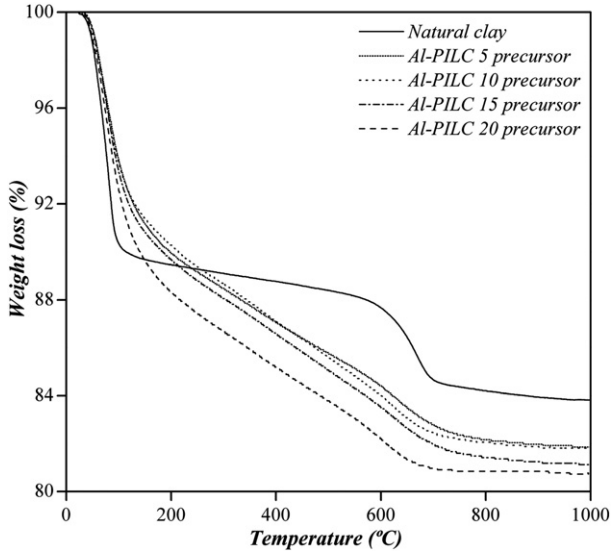

Fig. 4. Thermograms for natural clay mineral and PILC-precursors.

2.4. TB adsorption studies

The batch adsorption experiments were carried out in 10 mL centrifuge tubes by mixing 0.02 g of the sample with 8 mL of commercial TECTO solutions from 5 to 100 ppm. The pH of the dispersions was measured and was ever around 6.0, where the major specie is the neutral TB (from Fig. 2). Dispersions were continuously stirred for 24 h at 20 °C, which is enough time to reach the equilibrium according to previous studies (Roca Jalil et al., 2013). Then, the solution was separated from the adsorbent by centrifugation for 20 min at 6000 rpm using a Sorvall RC 5C centrifuge. TB concentrations in the resultant supernatant were determined by UV spectroscopy at 298 nm, corresponding to the TB maximum absorbance. A Hewlett-Packard 8453 UV–VIS spectrophotometer

Table 1
Textural properties data of adsorbents.

	S_{BET} (m^2 g^{-1})	V_T (cm^3 g^{-1})	$V_{\mu p}$ (cm^3 g^{-1})
Natural clay	64	0.09	0.01
Al-PILC 5	184	0.14	0.06
Al-PILC 10	279	0.17	0.10
Al-PILC 15	284	0.18	0.10
Al-PILC 20	286	0.16	0.10

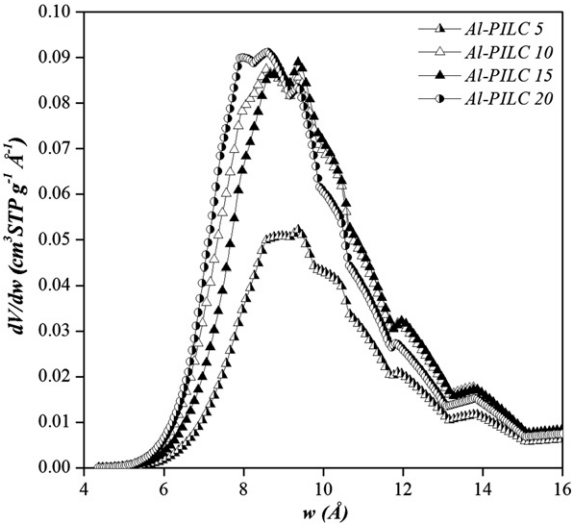

Fig. 6. PSD of PILC.

was used for these determinations. TB adsorption experiments were made in duplicate. The amount of TB adsorbed on the clays (q) was calculated from the initial and equilibrium TB concentrations, according to Eq. (1).

$$q = \frac{V\left(C_i - C_{eq}\right)}{w} \tag{1}$$

where V is the TB solution volume (L), C_i is the initial TB concentration (ppm), C_{eq} is the equilibrium TB concentration (ppm) and w is the mass of clay (g).

The solids obtained after centrifugation were dried at room temperature and studied by X-ray photoelectron spectroscopy (XPS) in order to evaluate the TB–adsorbent interaction.

TB adsorption equilibrium data were fitted to Langmuir, Freundlich and Sips isotherms models (Foo and Hameed, 2010; Frebrianto et al., 2009). The Langmuir isotherm model assumes a monolayer adsorption on a surface with a finite number of identical sites. This model supposes that all sites are energetically equivalent and there is no interaction among the adsorbed molecules. The mathematical expression of Langmuir isotherm model is shown in Eq. (2).

$$q = \frac{q_m k C_{eq}}{1 + k C_{eq}} \tag{2}$$

where q_m is the maximum amount adsorbed within a monolayer of adsorbate (mg g^{-1}) and k (ppm^{-1}) is the Langmuir dissociation constant, which is related to the adsorption energy.

The Freundlich equation is an empirical method that has been widely applied to adsorption on heterogeneous surfaces. This model uses a multi-site adsorption isotherm and its mathematical expression is defined in Eq. (3).

$$q = k_F C_{eq}^{1/n} \tag{3}$$

where k_F (L g^{-1}) and n (dimensionless) are the Freundlich characteristic constants, indicating the adsorption capacity and adsorption intensity, respectively.

The Sips equation is a combination of Langmuir and Freundlich equations. It is an empirical equation that assumes a heterogeneous surface with a number of active sites that interact with adsorbate molecule,

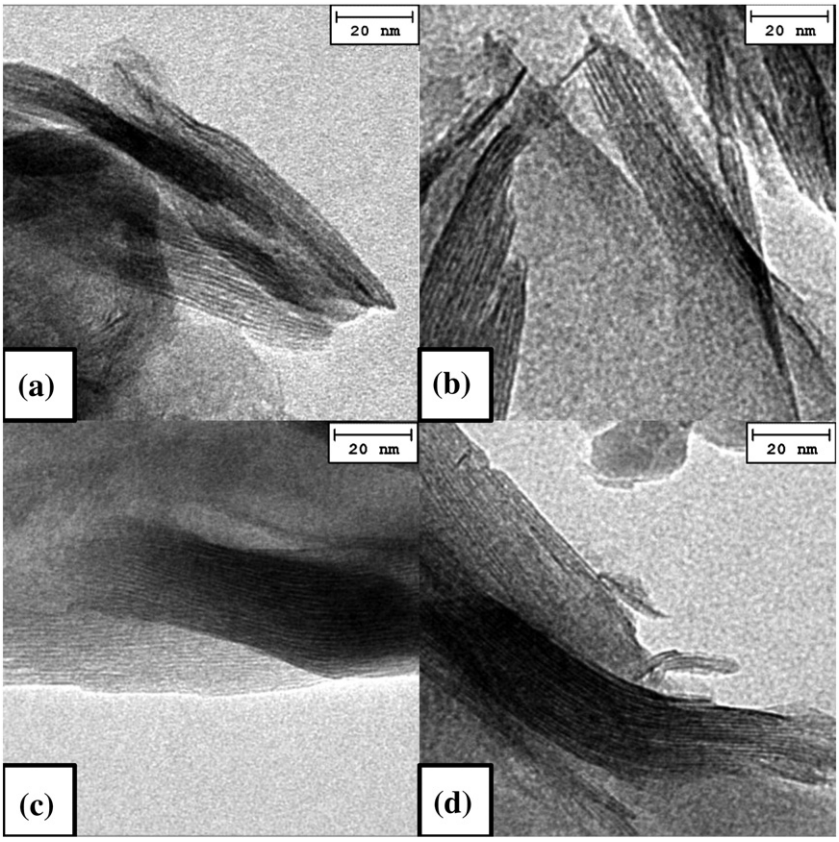

Fig. 7. Transmission electron micrograph for PILC where (a) Al-PILC 5, (b) Al-PILC 10, (c) Al-PILC 15 and (d) Al-PILC 20.

Table 2
Quantities of Al and Si in the adsorbents obtained by TEM/EDX analysis.

	% Al	% Si	Al/Si
Al-PILC 5	16.2	33.4	0.48
Al-PILC 10	15.1	28.7	0.53
Al-PILC 15	16.1	29.1	0.55
Al-PILC 20	17.0	29.7	0.57

without adsorbate–adsorbate interactions. The mathematical expression is shown in Eq. (4).

$$q = q_m \frac{\left(b \cdot C_{eq}\right)^{1/n}}{1 + \left(b \cdot C_{eq}\right)^{1/n}} \quad (4)$$

where q_m and C_{eq} have the same meanings as previously, b is a parameter related to the affinity of the adsorbate towards the surface and n is a parameter that represents the heterogeneity of the system.

3. Results and discussion

3.1. Adsorbents characterization

XRD patterns for natural and PILC are shown in Fig. 3. The obtained XRD pattern for the natural clay exhibits a basal distance (d_{001}) of 12.6 Å, typical of a natural sodium Mt, in accordance with its chemical analysis (Roca Jalil et al., 2013). Basal distances (d_{001}) around 18 Å were obtained for all PILC. Diffractograms did not show other structural changes in the PILC with respect to the starting material, since the peaks of the planes different to the basal remained unchanged. The incremental distance in 001 planes (Δd_{001}) was around 9 Å in comparison with the calcinated natural clay, for all obtained Al-PILC, this value is equivalent to the size of the aluminum Keggin cation reported by Bergaya et al. (2006). The increase in the basal distances could be assigned to the presence of aluminum oxide species within the interlayer, suggesting an effective pillarization process.

The TGA of the natural clay and the PILC precursors (before the calcination step) are shown in Fig. 4. The mass loss in all samples occurs in two steps. The first one is between 60 and 120 °C and is related to the loss of the physically adsorbed water on the natural clay. For the PILC precursors, this initial mass loss also includes the water associated to the oligocations. For the natural clay, the second mass loss step occurs around 600–700 °C and is due to the elimination of water from condensation of structural hydroxyls (Hedley et al., 2007). However, for the PILC the second step takes place in a broader temperature range, around 150–700 °C, where the mass loss is continuous and greater than that of the natural clay mineral and due to the loss of hydration water and dehydroxylation of the oligocation (Bergaya et al., 2006). Around 500 °C the aluminum oligocations lead to the formation of the aluminum oxide species in the interlayer, allowing the pillars to anchor.

N_2 adsorption–desorption isotherms at 77 K of the adsorbents are shown in Fig. 5. The natural clay mineral isotherm exhibits the typical features of Mt and can be classified as type IIb isotherm with an H3 type hysteresis loop according to the IUPAC classification (Rouquerol et al., 1999; Sing et al., 1984). This type of isotherm is related to mesoporous materials with aggregates of plate-like particles and agrees with the presence of the hysteresis loop. The low adsorption of N_2 at low relative pressures suggests a small contribution of micropores. The slight adsorption increase in the filling of mono-multilayer region at intermediate relative pressures indicates the presence of mesopores, which can be related to the turbostratic structure of the layers in the Mt. The increase of N_2 adsorption at high relative pressures corresponds to the presence of larger mesopores and can be associated to interparticle spaces.

The N_2 isotherms obtained for the PILC are a combination of type I and IIb isotherms, with H3 and H4-type hysteresis loops (Rouquerol et al., 1999; Sing et al., 1984). The type I isotherm results from the high increase of the N_2 adsorption at low relative pressures and it is associated to the higher presence of micropores in the PILC than in the natural clay. The adsorption at low relative pressures is similar for Al-PILC 10, 15 and 20 and lower for Al-PILC 5. The type IIb isotherm is related to the adsorption in the mono-multilayer region (from 0.05 to ca. 0.8 in relative pressures) which is similar to the natural clay. This behavior suggests that interstitial pores (Rouquerol et al., 1999; Sing et al., 1984) and the external structure of the natural clay are not affected by the pillarization process. The three first PILC show a hysteresis loop H3-type, similar to the natural clay, but the Al-PILC 20 has a hysteresis loop H4-type, indicating a more ordered structure than the other samples. Furthermore, the adsorption behavior of the Al-PILC 20 with respect to the other PILC does not show an increase at high relative pressures, typical for the nitrogen condensation in macropores, suggesting that the highest Al/clay ratio gives rise to a sample with only micro and mesopores in their structure.

The textural properties obtained from N_2-adsorption desorption isotherms are summarized in Table 1. An increase in the specific surface area (S_{BET}) for all PILC with regard to the natural clay mineral is observed. The increase in the S_{BET} and the micropore volume ($V_{\mu p}$) is explained by the behavior of N_2-adsorption isotherms at low relative pressures. Thus, an increase in the microporosity, higher than 43%, is obtained for all the PILC with respect to the natural clay mineral, evidencing the pillaring process. The V_T values agreed with the behavior of the

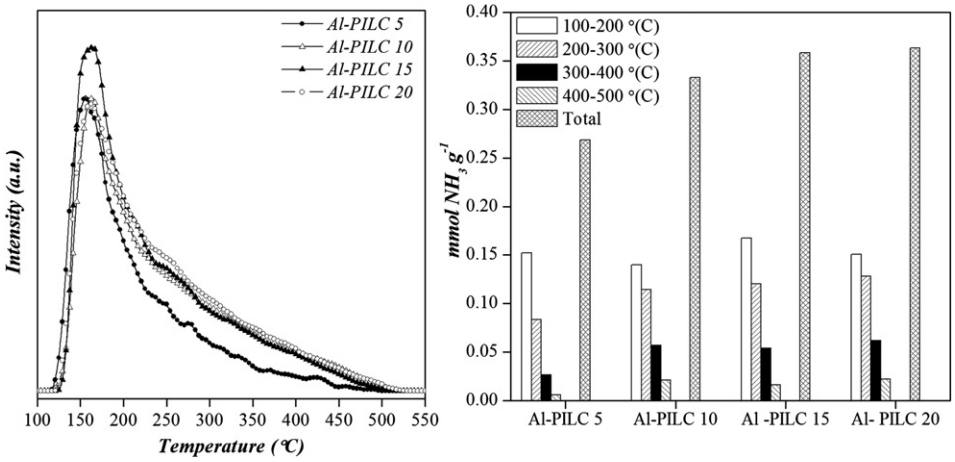

Fig. 8. Thermal programmed desorption of NH_3 for.

Table 3
Acidic properties of the adsorbents.

	Al-PILC 5	Al-PILC 10	Al-PILC 15	Al-PILC 20
Chemisorption (mmol NH_3 per g)	0.27	0.33	0.36	0.36
Number of acid centers per g	1.62×10^{20}	2.00×10^{20}	2.16×10^{20}	2.17×10^{20}
Number of acid centers per m^2	8.78×10^{17}	7.18×10^{17}	7.60×10^{17}	7.65×10^{17}

isotherms at high relative pressures. The Al-PILC 15 presents the highest value, suggesting a higher contribution of mesopores in this sample compared to Al-PILC 10 and Al-PILC 20 samples, because the micropore volumes were found to be similar among Al-PILC 10, Al-PILC 15 and Al-PILC 20.

PSD obtained for the PILC are shown in Fig. 6. The PSD were studied in the microporous region (pore size minor than 20 Å), where the development of microporosity due to the pillarization process could be observed. All materials have micropore sizes between 6 and 16 Å. When the Al/clay ratio is increased from 5 to 10, the micropore volume is increased, but the increments to 15 and 20 do not produce the same effect. The Al-PILC 10 and Al-PILC 15 present analogous behaviors, showing similar PSD. The Al-PILC 20 shows smaller pore sizes than the other PILC, suggesting greater pillar density within the interlayer, related with its high Al/clay ratio. The Al-PILC 5 has fewer micropore volume than the other materials indicating that at this Al/clay ratio, the pillarization is low.

The morphology of the PILC was evaluated by TEM (Fig. 7). The micrographs showed similar morphologies for the obtained Al-PILC. All materials show some ordered structures with longitudinal and face-to-face arrangements, similar to those reported for other PILC (Carriazo et al., 2007). Additionally, TEM/EDX analysis of the PILC samples (Table 2) shows an increase in the Al/Si ratio in accordance with the Al/clay ratio used in the synthesis. These results indicate that the Al-PILC 20 exhibits the highest aluminum content.

The acidic properties of the PILC (Fig. 8) were evaluated from NH_3-TPD experiments. In this figure, the ammonia desorbed vs the temperature is shown. The number of mmol of NH_3 chemisorbed was calculated from the amount of ammonia desorbed at temperatures higher than 100 °C. The acidic center number distribution for the temperature range of analysis is similar for all pillared samples. The acidity in PILC, mainly of Lewis-type is usually related to the presence of pillars and to the amount of aluminum incorporated with the oligocations (Lambert and Poncelet, 1997; Sapag and Mendioroz, 2001). However, there is also a contribution to the acidity due to the increase of the surface exposed when pillars are formed within the interlayer (Sapag and Mendioroz, 2001). The obtained results (Table 3) show that the amount of chemisorbed NH_3 increases with the aluminum content (Al/clay ratio) from 0.27 mmol NH_3 g^{-1} for the Al-PILC 5 to 0.36 mmol NH_3 g^{-1} for the Al-PILC 15 and 20 samples. However, if the amount of chemisorbed NH_3 is related to the S_{BET} of each material, the number of acid sites per m^2 of material is higher for the sample containing the least amount of aluminum, which is the Al-PILC 5 sample, because of its low S_{BET}.

3.2. Studies of TB adsorption

The adsorption isotherms obtained for TB on Al-PILC and their fits (lines) to Langmuir (Eq. (2)), Freundlich (Eq. (3)) and Sips (Eq. (4)) equations are shown in Fig. 9. The isotherms showed a similar adsorption behavior for all materials. The shape of the isotherms indicates L-type behavior according to the classification of Giles et al. (1974), suggesting the existence of high affinity between the adsorptive molecules and the surface solid (Giles et al., 1974; Konstantinou et al., 2000; Limousin et al., 2007). Furthermore, this type of isotherms indicates that the competition between the adsorptive and solvent molecules towards the surface of the solid is low. Table 4 compiles the fitting parameters as well as their correlation coefficients obtained by applying the above mentioned equations to the experimental data. Good fittings were obtained for PILC with Sips and Freundlich equations, which could indicate the existence of different adsorption sites on the surface of the solids. The values to the TB adsorption capacity of the solids obtained for both models showed the highest adsorption capacity for the Al-PILC 10 sample and the lowest for the Al-PILC

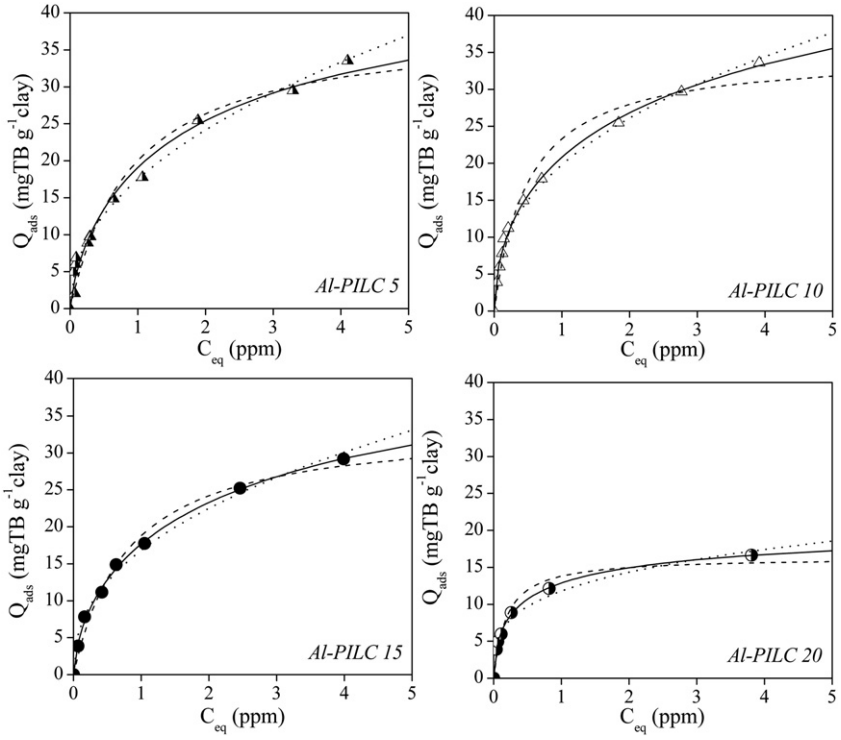

Fig. 9. Experimental isotherms (symbols) and Langmuir (dash), Freundlich (dot) and Sips (straight) eq. adjustments for the equilibrium adsorption data of TB on Al-PILC.

Table 4
Freundlich, Langmuir and Sips parameters for TB adsorption on aluminum PILC.

		Al-PILC 5	Al-PILC 10	Al-PILC 15	Al-PILC 20
Freundlich model	k_F (mg g^{-1}(ppm^{-1})^n)	17.50	19.80	16.82	11.78
	n	2.15	2.50	2.38	3.54
	R^2	0.98	0.99	0.99	0.98
Langmuir model	q_m (mg g^{-1})	38.47	34.98	33.99	16.35
	k (ppm^{-1})	1.08	1.99	1.23	5.39
	R^2	0.96	0.97	0.98	0.97
Sips model	q_m (mg g^{-1})	69.44	71.03	54.58	22.20
	b (ppm^{-1})	0.20	0.20	0.31	1.75
	n	1.51	1.82	1.57	1.74
	R^2	0.99	0.99	0.99	0.99

20 sample. Likewise, the value related to the heterogeneity of the systems (n) in the Sips equation was highest for the Al-PILC 10 sample. The b parameter is considered as a measure of the solids affinity towards TB. This parameter is higher for Al-PILC 20, indicating a higher affinity towards TB which could be related to the amount of aluminum incorporated. However, the number of acid sites per gram is similar for the Al-PILC 20 and Al-PILC 15 samples. This fact suggests that the high adsorbate–adsorbent affinity of the AL-PILC 20 sample is affected by the presence of the smaller micropores in this sample, compared to the other Al-PILC materials, as it is observed in Fig. 6.

The TB molecule has two pyridinic and one pyrrolic nitrogens, with reported binding energies of 399 eV and 400 eV, respectively (Casanovas et al., 1996). These values are in accordance with the results reported by Lombardi et al. (2006), who found that the N1*s* spectrum of pure TB shows only one peak around 399 eV. Consequently, changes in the chemical environment of TB nitrogens can be studied by means of XPS in order to study the adsorbate–adsorbent interactions. Taking into account that the electrons of the pyrrolic nitrogen are involved in the aromatic ring, the pyridinic nitrogens are expected to present a major Lewis basicity. Günert and Schlögl (2004) reported that pyridinic nitrogen interacting with Lewis acid sites shows a signal at around 401 eV. In this sense, the study of the evolution of XPS signals at 399 and 401 eV could indicate the proportion of pyridinic nitrogen that is interacting with the pillars in the adsorbate–adsorbent system. Therefore, the peak around 399 eV could be related to pyridinic nitrogen of physisorbed TB, and the peak around 401 eV could be related to pyridinic nitrogen of chemisorbed TB.

Fig. 10 shows the N1*s* spectra obtained for TB-PILC complexes which were decomposed into two components at 399.3 eV and 401.1 eV. This figure shows that the TB–Al-PILC 5, 10 and 15 complexes present the highest contribution of the peak at 401 eV, indicating a higher contribution of chemisorbed TB in these three samples. However, in the TB–Al PILC 20 complex the intensity of the peak around 399 eV is higher; indicating that TB molecules on Al-PILC 20 are mainly physisorbed. Table 5 summarizes the XPS binding energies and the proportion of the previously mentioned nitrogen species in the different TB–Al PILC complexes, calculated as the ratio between the areas under the two peaks studied. By comparing this ratio, it is corroborated the behavior observed in Fig. 10, where the less proportion of chemisorbed TB is obtained for the Al-PILC 20 sample. This phenomenon could be associated with the attraction potential within small micropores and the fact that in these type of pores TB molecules are highly attracted, but could not be allowed to orientate freely, diminishing the Lewis interactions of adsorbed TB molecules with the pillars. Also, the existence of small

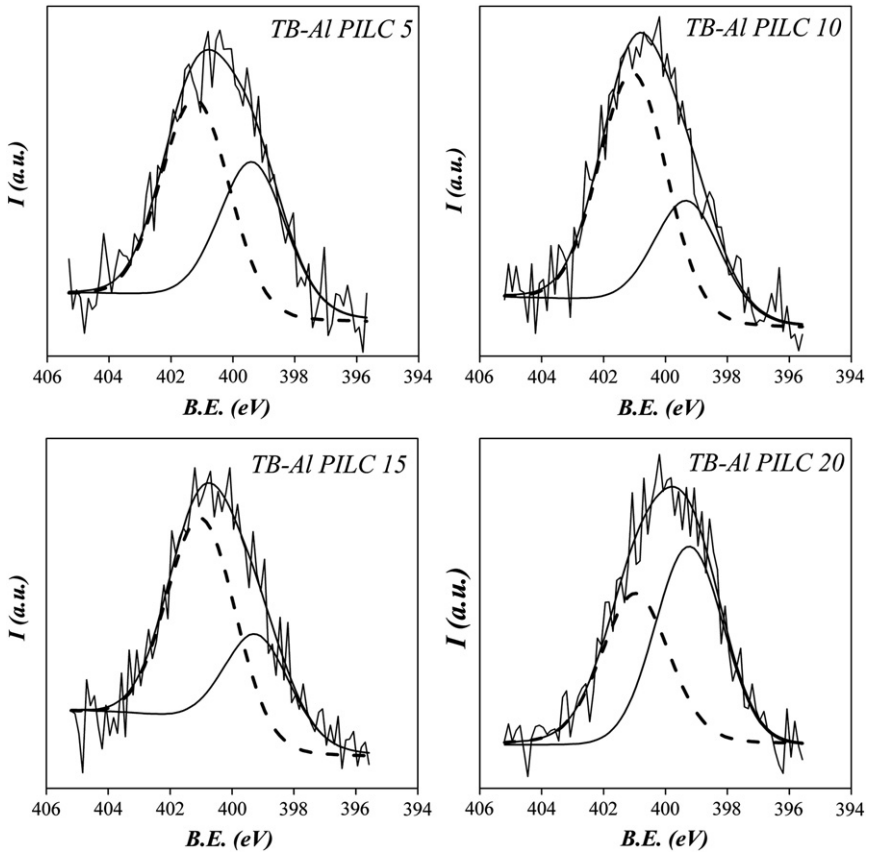

Fig. 10. N1*s* core level spectra for TB-Al PILC complexes.

Table 5
XPS data for the TB-PILC complexes (N 1*s* binding energy and percentages for each specie).

TB-pillared clay complexes	N 1 *s* binding energy (eV)	
	TB-physisorbed	TB-chemisorbed
Al-PILC 5	399.3 (44.5%)	401.2 (55.5%)
Al-PILC 10	399.3 (34.9%)	401.1 (65.1%)
Al-PILC 15	399.2 (36.7%)	401.0 (63.3%)
Al-PILC 20	399.2 (53.7%)	400.9 (46.3%)

micropores in the porous system of Al-PILC 20 can obstruct the access of some TB molecules. This pore-blocking phenomenon could explain the lowest TB adsorption observed in this sample, in spite of the fact that it presents the highest S_{BET}, the highest amount of acid sites per gram, and similar $V_{\mu p}$ to the other PILC samples.

On the other hand, the other PILC samples show higher proportion of chemisorbed TB than physisorbed TB, suggesting that most of the TB molecules adsorbed in these samples are interacting with the Lewis acid sites of the PILC samples. This phenomenon could be assigned to the highest accessibility of TB to the porous structure in these samples, due to the presence of larger pore sizes, as can be appreciated in the PSD of Fig. 6. Also, it is observed that the proportion of physisorbed TB is higher in the Al-PILC 5 sample than in Al-PILC 10 and Al-PILC 15 ones, perhaps due to its lower amount of pillars.

These results show that the PSD is a critical parameter in TB adsorption capacity of PILC materials in the conditions studied. It is observed that the PSD could be affecting not only the accessibility of TB to the porous structure, but also the mechanism of TB adsorption.

Moreover, it was found that the best relationship between pore size, pillar density and surface properties was obtained for Al-PILC 10, which shows the highest TB adsorption capacity.

4. Conclusions

This work shows that Al-PILC could be good adsorbents for fungicides such as TB from aqueous media. It was found that TB adsorption capacity of the Al-PILC is strongly dependent of the porous structure of this type of materials. Also, it was observed that the Al/clay ratio used in the synthesis of PILC materials affects the porous structure and the surface properties of the materials obtained. The different PSD obtained for the Al-PILC materials with different Al/clay ratios showed that the materials with the highest aluminum content developed the smallest pore sizes. The development of this kind of microporosity is not recommended for TB adsorption, because the presence of narrow micropores can block the access of TB molecule to some adsorption sites, diminishing the TB adsorption capacity.

XPS studies showed that TB can be physisorbed or chemisorbed in PILC materials, and that the proportion of these species in adsorbed TB depends on the Al/clay ratio and the PSD of the materials. It was found that the highest TB adsorption capacity was obtained for Al-PILC 10, showing that this material has the best relationship between the pillar density and the surface properties.

Acknowledgments

The authors gratefully acknowledge the Universidad Nacional San Luis, CONICET, ANPCyT (Agencia Nacional de Promoción Científica y Tecnológica), Universidad Nacional del Comahue and Universidad de Málaga for their financial support.

References

Bergaya, F., Aouad, A., Mandalia, T., 2006. Pillared clays and clay minerals. In: Bergaya, F., Theng, B.K.G., Lagaly, G. (Eds.), Handbook of Clay Science — Developments in Clay Science. Elsevier, Amsterdam, pp. 393–421.

Carriazo, J.G., Centeno, M.A., Odriozola, J.A., Moreno, S., Molina, R., 2007. Effect of Fe and Ce on Al-pillared bentonite and their performance in catalytic oxidation reactions. Appl. Catal. A 317, 120–128.

Casanovas, J., Ricart, J.M., Rubio, J., Illas, F., Jiménez-Mateos, J.M., 1996. Origin of the large N1s binding energy in X-ray photoelectron spectra of calcined carbonaceous materials. J. Am. Chem. Soc. 118, 8071–8076.

Cool, P., Vansant, E.F., 1998. Pillared clays: preparation, characterization and applications. In: Karge, H.G., Weitkamp, J. (Eds.), Molecular Sieves — Science and Technology: Synthesis. Springer-Verlag, Berlin, pp. 265–288.

Crini, G., 2006. Non-conventional low-cost adsorbents for dye removal: a review. Bioresour. Technol. 97, 1061–1085.

Del Piero, S., Melchior, A., Polese, P., Portanova, R., Tolazzi, M., 2006. A novel multipurpose Excel tool for equilibrium speciation based on Newton–Raphson method and on a hybrid genetic algorithm. Ann. Chim. 96, 29–49.

Foo, K.Y., Hameed, B.H., 2010. Insights into the modeling of adsorption isotherm systems. Chem. Eng. J. 156, 2–10.

Frebrianto, J., Kosasih, A., Sunarso, J., Ju, Y., Indraswati, N., Ismadji, S., 2009. Equilibrium and kinetic studies in adsorption of heavy metals using biosorbent: a summary of recent studies. J. Hazard. Mater. 162, 616–645.

Gil, A., Korili, S.A., Vicente, M.A., 2008. Recent advances in the control and characterization of the porous structure of pillared clay catalysts. Catal. Rev. 50, 153–221.

Gil, A., Assis, F.C.C., Albeniz, S., Korili, S.A., 2011. Removal of dyes from wastewaters by adsorption on pillared clays. Chem. Eng. J. 168, 1032–1040.

Giles, C.H., D`Silva, A.P., Easton, I.A., 1974. A general treatment and classification of the solute adsorption isotherm. Part II. Experimental interpretation. J. Colloid Interface Sci. 47, 766–778.

Günert, W., Schlögl, R., 2004. Photoelectron spectroscopy of zeolites. In: Karge, H.G., Weitkamp, J. (Eds.), Molecular Sieves — Science and Technology: Characterization I. Springer-Verlag, Berlin, pp. 467–515.

Hedley, C.B., Yuan, G., Theng, B.K.G., 2007. Thermal analysis of montmorillonites modified with quaternary phosphonium and ammonium surfactants. Appl. Clay Sci. 35, 180–188.

Hou, M.-F.-, Ma, C.-X., Zhang, W.D., Tang, X.-Y., Fan, Y.-N., Wan, H.-F., 2011. Removal of rhodamine B using iron pillared bentonite. J. Hazard. Mater. 186, 118–1123.

Kloprogge, J.T., 1998. Synthesis of smectites and porous pillared clay catalysts: a review. J. Porous Mater. 5, 5–41.

Konstantinou, I.K., Albanis, T.A., Petrakis, D.A., Pomonis, P.J., 2000. Removal of herbicides from aqueous solutions by adsorption on Al-pillared clays, Fe–Al pillared clays and mesoporous alumina aluminum phosphates. Water Res. 34, 3123–3136.

Lambert, J.F., Poncelet, G., 1997. Acidity in pillared clays: origin and catalytic manifestations. Top. Catal. 4, 43–56.

Limousin, G., Gaudet, J.P., Charlet, L., Szenlnect, S., Barthes, V., Krimissa, M., 2007. Sorption isotherms: a review on physical bases, modeling and measurement. Appl. Geochem. 22, 249–275.

Lombardi, B., Baschini, M.T., Torres Sanchez, R.M., 2003. Optimization of parameters and adsorption mechanism of thiabendazole fungicide by a montmorillonite of North Patagonia Argentina. Appl. Clay Sci. 24, 43–50.

Lombardi, B.M., Torres Sánchez, R.M., Eloy, P., Genet, M., 2006. Interaction of thiabendazole and benzimidazole with montmorillonite. Appl. Clay Sci. 33, 59–65.

Manohar, D.M., Noelite, B.F., Anirudhan, T.S., 2005. Removal of vanadium (IV) from aqueous solutions by adsorption process with aluminum-pillared bentonite. Ind. Eng. Chem. Res. 44, 6676–6684.

Mishael, Y.G., Rytwo, G., Nir, S., Crespin, M., Annabi-Bergaya, F., Van Damme, H., 1999. Interactions of monovalent organic cations with pillared clays. J. Colloid Interface Sci. 209, 123–128.

Molu, Z.B., Yurdakoc, K., 2010. Preparation and characterization of aluminum pillared K10 and KSF for adsorption of trimethoprim. Microporous Mesoporous Mater 127, 50–60.

Oliveira, L.C.A., Lago, R.M., Fabris, J.D., Sapag, K., 2008. Catalytic oxidation of aromatic VOCs with Cr or Pd-impregnated Al-pillared bentonite: byproduct formation and deactivation studies. Appl. Clay Sci. 39, 218–222.

Polubesova, T., Nir, S., Gerstl, Z., Borisover, M., Rubin, B., 2002. Imazaquin adsorbed on pillared clay and crystal violet–montmorillonite complexes for reduced leaching in soil. J. Environ. Qual. 31, 1657–1664.

Roca Jalil, E., 2010. Desarrollo de Arcillas Pilareadas con Al a partir de una bentonita natural de la Norpatagonia Argentina para la remoción de tiabendazol. (MSc. Thesis) Universidad Nacional de San Luis, San Luis, Argentina.

Roca Jalil, M.E., Vieira, R., Azevedo, D., Baschini, M., Sapag, K., 2013. Improvement in the adsorption of thiabendazole by using aluminum pillared clays. Appl. Clay Sci. 71, 55–63.

Romero-Pérez, A., Infantes-Molina, A., Jiménez-López, A., Roca Jalil, E., Sapag, K., Rodríguez-Castellón, E., 2012. Al-pillared montmorillonite as a support for catalysts based on ruthenium sulfide in HDS reactions. Catal. Today 187, 88–96.

Rouquerol, J., Rouquerol, F., Sing, K., 1999. Adsorption by Powders and Porous Solids, Principles, Methodology and Applications. Academic Press, New York.

Sapag, K., Mendioroz, S., 2001. Synthesis and characterization of micro-mesoporous solids: pillared clays. Colloids Surf. A 187–188, 141–149.

Sing, K.S.W., Everett, D.H., Haul, R.A.W., Moscou, L., Pierotti, R.A., Rouquerol, J., Siemieniewska, T., 1984. Reporting physisorption data for gas/solid systems with special reference to the determination of surface area and porosity. Pure Appl. Chem. 57, 603–619.

Tian, S., Jiang, P., Ning, P., Su, Y., 2009. Enhanced adsorption of phosphate from water by mixed lanthanum/aluminum pillared montmorillonite. Chem. Eng. J. 151, 141–148.

Tway, P., Love, L.J.C., 1982. Effects of excited-state prototropic equilibria on the fluorescence energies of benzimidazole and thiabendazole homologues. J. Phys. Chem. 86, 5227–5230.
Undabeytia, T., Nir, S., Rubin, B., 2000. Organo-clay formulations of the hydrophobic herbicide norflurazon yield reduced leaching. J. Agric. Food Chem. 48, 4767–4773.
Vicente, M.A., Gil, A., Bergaya, F., 2013. Pillared clays and clay minerals. In: Bergaya, F., B.K.G., Lagaly, G. (Eds.), Handbook of Clay Science. Part A: Fundamentals. Elsevier, Amsterdam. ISBN: 978-0-08-098259-5, pp. 393–421.
Wang, C.J., Li, Z., Jiang, W.T., 2011. Adsorption of ciprofloxacin on 2:1 dioctahedral clay minerals. Appl. Clay Sci. 53, 723–728.